

Comparison of Electromagnetic Interference Potential of Integrated Logic Circuits AVC, GTLP, BTL, and LVDS

Johannes Huchzermeier
Standard Linear & Logic

ABSTRACT

Although ideal digital signals are square waves, in practice, these signals have a trapezoidal shape that, with period duration (frequency) of the recurrent signal, determines their electromagnetic-interference potential. Effective electromagnetic radiation depends to signal characteristics and circuit-board design.

This application report compares different technologies for data transmission with respect on their electromagnetic-interference behavior. Fourier-series development is used to compare spectral content of output signals and harmonics from AVC, GTLP, BLT, and LVDS technologies. Amplitude spectra of four representative devices, measured using a transverse electromagnetic mode measurement cell, are presented.

Contents

Fundamental Structure of Periodic Signals	4
Signal Form Determines Electromagnetic Radiation That Influences the Layout	4
Fourier-Series Development	6
Measurement of the Harmonic Contents of a Digital Signal	13
Measurement of the Amplitude Spectrum in the TEM Cell	13
Measurement Boards	14
Measurement Results	15
AVC16244	16
FB2033A	19
GTLPH1655	22
LVDS31	27
Summary	29
Glossary	30
Bibliography	31

List of Figures

1	Example of an Antenna Loop (Basic Loop) on a Circuit Board	5
2	Time Curve for a Trapezoidal Signal	7
3	Spectrum for a Triangular Signal, Signal and Components in Time Domain	9
4	Spectrum for a Triangular Signal (Signal From Figure 3 in the Frequency Domain)	9
5	Spectrum for a Trapezoidal Signal, Signal and Components in Time Domain, Same Signal in Frequency Domain	10
6	Spectrum for a Trapezoidal Signal (Signal From Figure 5 in Frequency Domain)	10
7	Comparison of Various Technologies' Harmonics	12
8	Measurement of the Electromagnetic Field Using a TEM Cell	13
9	Layer Structure of Measurement Boards for the TEM Cell	14
10	Input and Output Signals of AVC16244, $V_{CC} = 3.3$ V, $f = 10$ MHz, Input Signal LVTTTL $t_{r,f} = 10$ ns; Output Signal LVTTTL	16
11	Input and Output Signals of AVC16244, $V_{CC} = 3.3$ V, $f = 10$ MHz, Input Signal LVTTTL $t_{r,f} = 2$ ns; Output Signal LVTTTL	16
12	Spectrum Measured in the TEM Cell, AVC16244, $V_{CC} = 3.3$ V, $f = 10$ MHz	17
13	Input and Output Signals of AVC16244, $V_{CC} = 1.2$ V, $f = 10$ MHz; Input Signal 1.2 V, $t_{r,f} = 10$ ns; Output Signal 1.2-V CMOS	17
14	Input and Output Signals of AVC16244, $V_{CC} = 3.3$ V, $f = 10$ MHz, Input Signal 1.2 V, $t_{r,f} = 2$ ns; Output Signal 1.2-V CMOS	18
15	Spectrum Measured in the TEM Cell, AVC16244, $V_{CC} = 1.2$ V, $f = 10$ MHz	18
16	Input and Output Signals of FB2033A, $f = 10$ MHz, Input Signal LVTTTL, $t_{r,f} = 2$ ns; Output Signal BTL	19
17	Input and Output Signals of FB2033A, $f = 10$ MHz, Input Signal LVTTTL, $t_{r,f} = 10$ ns; Output Signal BTL	19
18	Spectrum Measured in the TEM Cell, FB2033A, $f = 10$ MHz, Input Signal BTL; Output Signal LVTTTL	20
19	Input and Output Signals of FB2033A, $f = 10$ MHz; Input Signal BTL, $t_{r,f} = 2$ ns; Output Signal LVTTTL	20
20	Input and Output Signals of FB2033A, $f = 10$ MHz, Input Signal BTL, $t_{r,f} = 10$ ns; Output Signal LVTTTL	21
21	Spectrum Measured in the TEM Cell FB2033A, $f = 10$ MHz, Input Signal LVTTTL; Output Signal BTL	21
22	Input and Output Signals of GTLPH1655, $f = 10$ MHz, Input Signal LVTTTL, $t_{r,f} = 2$ ns; Output Signal GTL+ With Slow Edge Rate	22
23	Input and Output Signals of GTLPH1655, $f = 10$ MHz, Input Signal LVTTTL, $t_{r,f} = 10$ ns, Output Signal GTL+ With Slow Edge Rate	23
24	Spectrum Measured in the TEM Cell, GTLPH1655 $f = 10$ MHz, Input Signal LVTTTL; Output Signal GTL+ With Slow Edge Rate	23
25	Input and Output Signal of GTLPH1655, $f = 10$ MHz, Input Signal LVTTTL, $t_{r,f} = 2$ ns; Output Signal GTL+ With Fast Edge Rate	24
26	Input and Output Signals of GTLPH1655, $f = 10$ MHz, Input Signal LVTTTL, $t_{r,f} = 10$ ns; Output Signal GTL+ With Fast Edge Rate	24
27	Spectrum Measured in the TEM Cell for GTLPH1655, $f = 10$ MHz, Input Signal LVTTTL; Output Signal GTL+ With Fast Edge Rate	25
28	Input and Output Signals of GTLPH1655, $f = 10$ MHz, Input Signal GTL+, $t_{r,f} = 10$ ns; Output Signal GTL+ LVTTTL	25
29	Input and Output Signal of GTLPH1655, $f = 10$ MHz, Input Signal GTL+, $t_{r,f} = 2$ ns; Output Signal LVTTTL	26

30	Spectrum Measured in the TEM Cell for GTLPH1655, $f = 10$ MHz, Input Signal GTL+; Output Signal LVTTTL	26
31	Input and Output Signals of LVDS31, $f = 10$ MHz, TTL Input Signal, $t_{r,f} = 10$ ns; Output Signal LVDS	27
32	Input and Output Signals of LVDS31, $f = 10$ MHz, Input Signal TTL, $t_{r,f} = 2$ ns; Output Signal LVDS	28
33	Spectrum Measured in the TEM Cell for LVDS31, $f = 10$ MHz, Input Signal TTL; Output Signal LVDS	28

List of Tables

1	Comparison of Signal Levels Among Various Technologies	11
2	Calculated Amplitudes of Harmonics for Various Technologies	12

Fundamental Structure of Periodic Signals

Digital data transmission ideally is based on square-wave signals. However, in practice, signals have a limited slope because a certain time is required for the transition from one logic state to another. Therefore, it is realistic to study trapezoidal signal patterns with different signal edge rates that are due to various load conditions at the driver output.

When referring to the speed of a digital system, for example, that of a personal computer (PC), normally we mean its clock frequency. Clock frequency is the highest-frequency signal of an asynchronous system. In a synchronous system, all data or control signals relate to a consistent system clock. The higher the selected frequency for the system clock, the faster the system is, but, also, the higher is the clocked signal's electromagnetic interference potential for the same signal rise and the same signal form.

A periodic signal can be displayed both in the time range and in the frequency range.

When plotting the current or voltage curve over time, we obtain function $f(t) = u(t), i(t)$, respectively, in the time range. The signal can be displayed in the time range using an oscilloscope.

In the frequency range, we plot voltage or current components over frequency. Here, sine-wave signals of various frequencies and amplitudes are plotted and their total produces the signal. Amplitudes also are designated as spectrum lines that can arise as multiples of the base frequency. By measurement, a signal's frequency spectrum can be detected using a spectrum analyzer.

It is possible to comment on frequency proportions and, thus, on electromagnetic interference potential, if these prerequisites are known:

- Signal form, i.e., in the case of digital signals, the signal's slope and amplitude
- Frequency, i.e., the period duration of the recurrent signal

Each periodic signal form can be generated by superimpositions of sine-wave functions of differing frequencies and amplitudes. Fourier-series development provides the basis for calculating a signal's spectrum components.

Signal Form Determines Electromagnetic Radiation That Influences the Layout

Effective electromagnetic radiation is not determined by signal form and frequency alone. The signal determines only the interference potential. The three components of the interference signal source, the interference channel, and the interference signal drain are inseparably involved in electromagnetic radiation.

Interference signal sources within a system are diverse and can, for example, result from line reflections due to mismatching, crosstalk between two adjacent signal lines, current peaks arising at the moment of switching due to totem-pole output stages, etc.

Circuit layout exerts a decisive influence on how effectively the generated faults can be irradiated or propagated. The benefit arising from data transport between a driver output and the input of the subsequent stage can be offset, if circuit design is poor, by interference characteristics with the effective-antenna effect in the cable connection.

In addition to cable connection length, the enclosed area between the data line (between the transmitter and the receiver) and the signal return path via the GND connection (between the receiver and the transmitter) can have a decisive influence on the level of propagation or radiation of electromagnetic waves. This problem is illustrated in Figure 1.

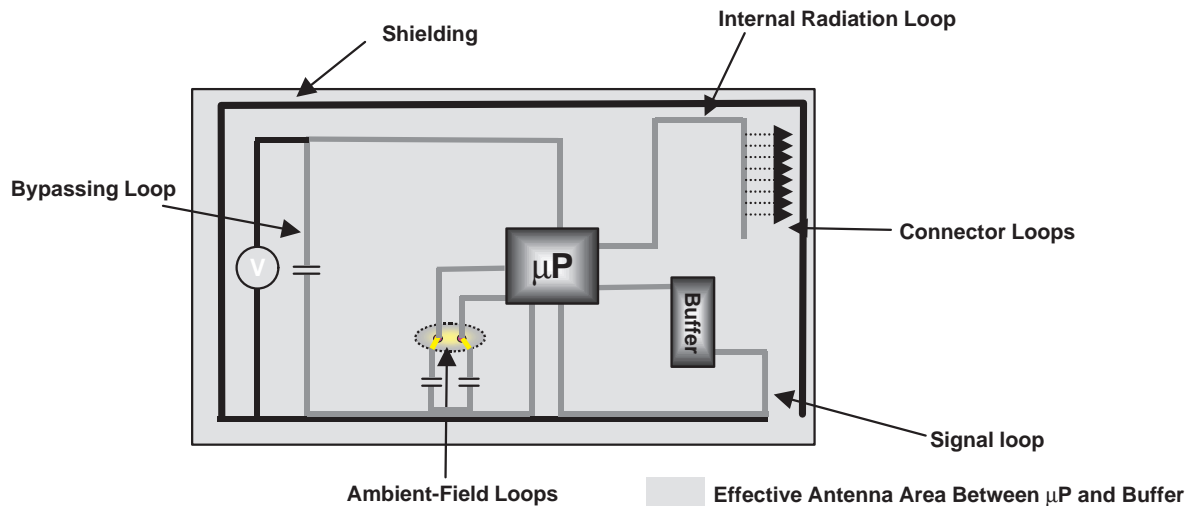


Figure 1. Example of an Antenna Loop (Basic Loop) on a Circuit Board

In this context, particular emphasis is placed on the signal loop that is set up between the output of the microprocessor (μP) through the buffer module input, through the ground connection of the buffer module to the system ground, and through the system ground back to the microprocessor ground. Figure 1 also contains further examples of basic loops that have a possible antenna effect.

The highest level of effectiveness for radiation and propagation occurs when an interference source is transmitting on a frequency whose quarter wavelength corresponds to the line length in a given layout. For example, for a loop length of 10 cm, an antenna's transmission frequency is 749.5 MHz.

The objective is not simply to utilize a technology that possesses the lowest possible interference potential. Developers also should ensure that the antenna effect of circuit-board layout is minimized by using appropriate line lengths and, for example, by additional screening in the form of ground lines or ground planes, to ensure the lowest-impedance path possible for interference or faults.

Fourier-Series Development

Using the example of the trapezoidal signal in digital systems, the signal is broken down into its spectral components, using Fourier-series development.

The conclusion of theoretical considerations is represented by the comparison of the spectra of a triangular signal and of a typical digital signal, both having equal amplitude and fundamental frequency. Various technologies for data transmission at 5 V, 3.3 V, 2.1 V, and 1.5 V are compared regarding their spectral contents. For this purpose, the Fourier-series development was applied to the nominal-output signals of each technology. The typical edge rate and signal rise time for the corresponding technology has been calculated for 10 MHz.

The prerequisite for Fourier-series development is that it should relate to an unequivocal continuous-section periodic function whose base period is T_0 in the interval of $\langle 0, T_0 \rangle$.

The basic formula for Fourier-series development is:

$$f(t) = \frac{A_0}{2} + \sum_{n=1}^{\infty} [A_n \cos(n\omega_0 t) + B_n \sin(n\omega_0 t)] \quad (1)$$

Where:

$$\text{Radian frequency, } \omega_0 = \frac{2\pi}{T_0}$$

T_0 = signal period duration

Equation 1 shows that the complete time signal is made up of an identical proportion and an increment of the sine and cosine functions of multiples of the base frequency. The purpose of Fourier-series development is to determine coefficients A_n and B_n .

By definition, the general form of the coefficients is:

$$A_0 = \frac{2}{T_0} \int_{t_0}^{t_0+T_0} f(t) dt \quad (2)$$

$$A_n = \frac{2}{T_0} \int_{t_0}^{t_0+T_0} f(t) \cos(n\omega_0 t) dt \quad (3)$$

$$B_n = \frac{2}{T_0} \int_{t_0}^{t_0+T_0} f(t) \sin(n\omega_0 t) dt \quad (4)$$

The study can be reduced to the primary period where $t_0 = 0$. Figure 2 illustrates the signal path of a trapezoidal signal that changes in the borderline cases of $t_1 = 0$ to a square-wave signal, and, where $t_1 = T/4$, the signal changes into a triangular signal.

A Fourier series is developed in a general form for the function $u(t)$ as follows:

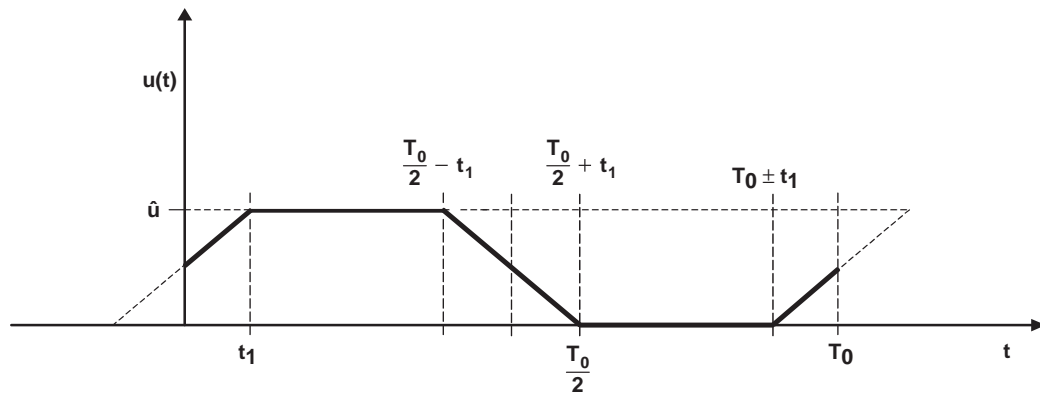


Figure 2. Time Curve for a Trapezoidal Signal

Initially, the signal is defined by equations 5 through 9 in the five function sections of the basic period:

$$u(t) = \frac{\hat{u}}{2} + \frac{\hat{u}}{2t_1}t \quad (5)$$

Where:

$$0 < t \leq t_1$$

$$u(t) = \hat{u} \quad (6)$$

Where:

$$t_1 < t \leq \frac{T_0}{2} - t_1$$

$$u(t) = \hat{u} - \frac{\hat{u}}{2t_1} \left[t - \left(\frac{T_0}{2} - t_1 \right) \right] \quad (7)$$

Where:

$$\frac{T_0}{2} - t_1 < t \leq \frac{T_0}{2} + t_1$$

$$u(t) = 0 \quad (8)$$

Where:

$$\frac{T_0}{2} + t_1 < t \leq T_0 - t_1$$

$$u(t) = \frac{\hat{u}}{2t_1} \left[t - (T_0 - t_1) \right] \quad (9)$$

Where:

$$T_0 - t_1 < t \leq T_0$$

Next, the functions of equations 5 through 9 for $f(t)$ are substituted in equations 1 through 3 and partially integrated. For the factor A_0 , this gives the value $\hat{u}/2$, which corresponds to the dc content of the signal.

Components A_n do not appear. The absence of cosine components, A_n , is typical for so-called odd functions, which are discrete symmetrical to the point of origin, reduced by, or added with, any dc component.

Components B_n result in:

$$B_n = \left| \sin\left(\frac{n\pi}{2}\right) \right| \times \frac{4\hat{u}}{\pi\varphi} \times \frac{1}{n^2} \times \sin(n\varphi) \quad (10)$$

Where:

$$\varphi = 2\pi \frac{t_1}{T_0}$$

The following total is obtained as the Fourier series for the trapezoidal signal in Figure 2:

$$u(t) = \frac{4\hat{u}}{\pi\varphi} \left[\frac{1}{12} \times \sin(\varphi) \sin(\omega_0 t) + \frac{1}{32} \times \sin(3\varphi) \sin(3\omega_0 t) + \frac{1}{52} \times \sin(5\varphi) \sin(5\omega_0 t) + \dots \right] \quad (11)$$

In the special case where $t_1 = T_0/4$ (see Figure 3), a triangular curve results. The Fourier series then results in:

$$u(t) = \frac{8\hat{u}}{\pi\varphi} \left[\frac{1}{12} \times \sin(\omega_0 t) - \frac{1}{32} \sin(3\omega_0 t) + \frac{1}{52} \times \sin(5\omega_0 t) - \dots + \dots \right] \quad (12)$$

From equations 11 and 12, the amplitudes of the spectrum lines of a triangular signal decrease far more rapidly than those of a trapezoidal signal.

Figures 4 and 6 show the frequency spectra for a trapezoidal signal and for a triangular signal whose base frequency is $f_0 = 10$ MHz, as calculated with equations 11 and 12. Amplitudes are stated in μVdB .

While the spectrum for the triangular signal illustrated on the left decreases constantly at 40 dB per decade, the calculated spectrum for the trapezoidal signal shows two ranges:

1. Up to a cutoff frequency, spectrum components descend by 20 dB per decade.
2. Above the cutoff frequency, components decay at 40 dB per decade.

The cutoff frequency is determined by the signal's edge rate and can be calculated using equation 13.

$$f_{\text{cutoff}} = \frac{1}{\pi \times t_{r,f}} \quad (13)$$

Where:

- t_r = rising edge
- t_f = falling edge

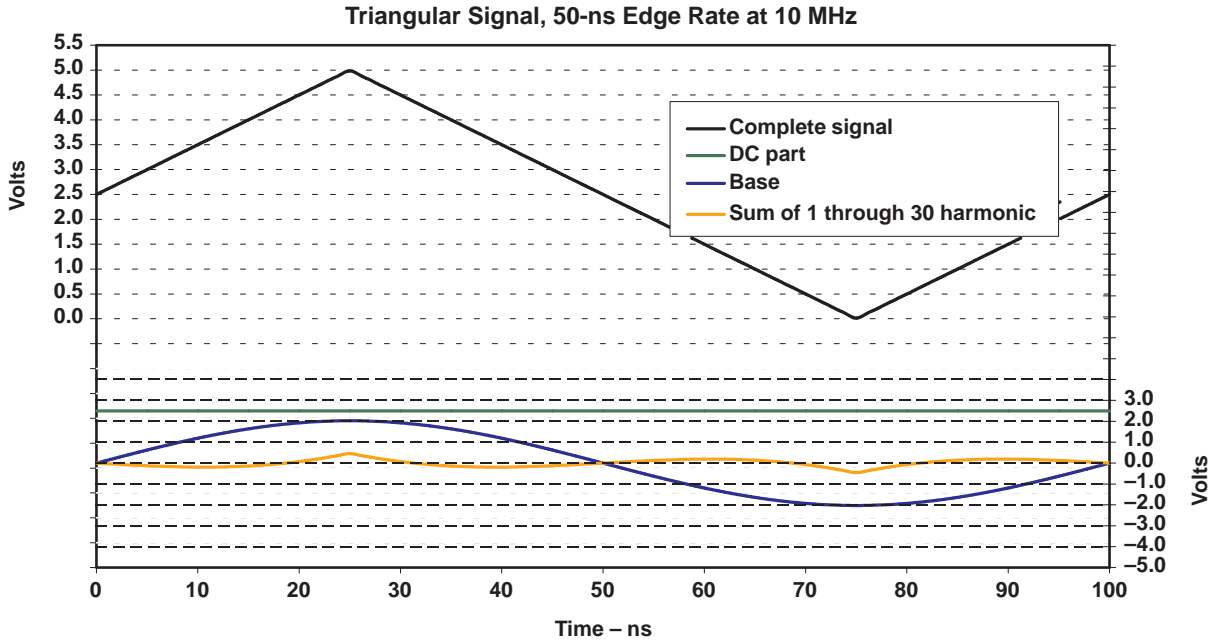


Figure 3. Spectrum for a Triangular Signal, Signal and Components in Time Domain

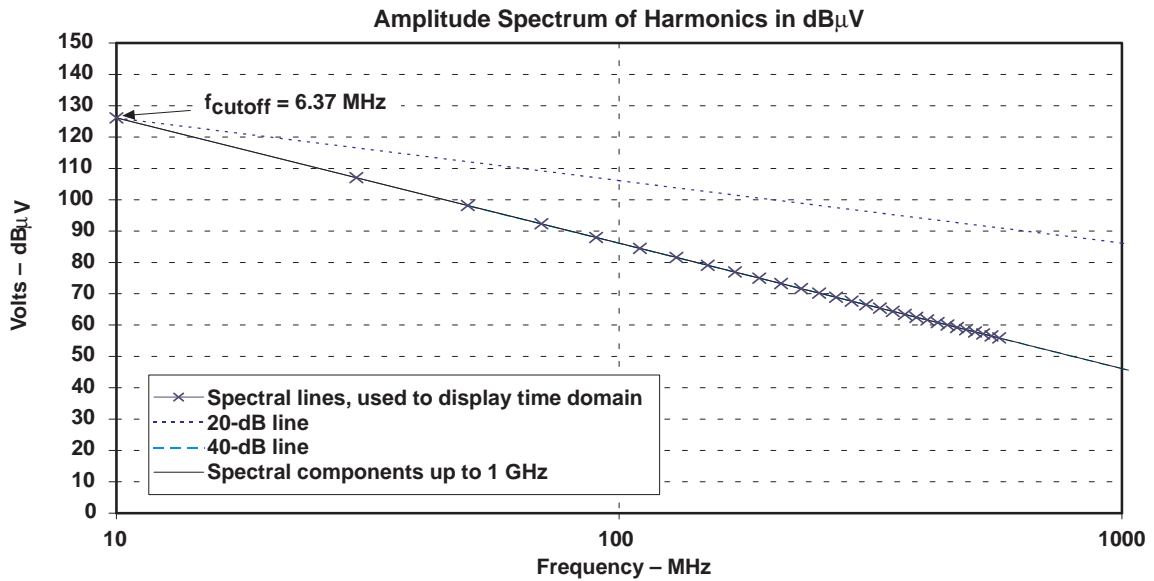


Figure 4. Spectrum for a Triangular Signal (Signal From Figure 3 in the Frequency Domain)

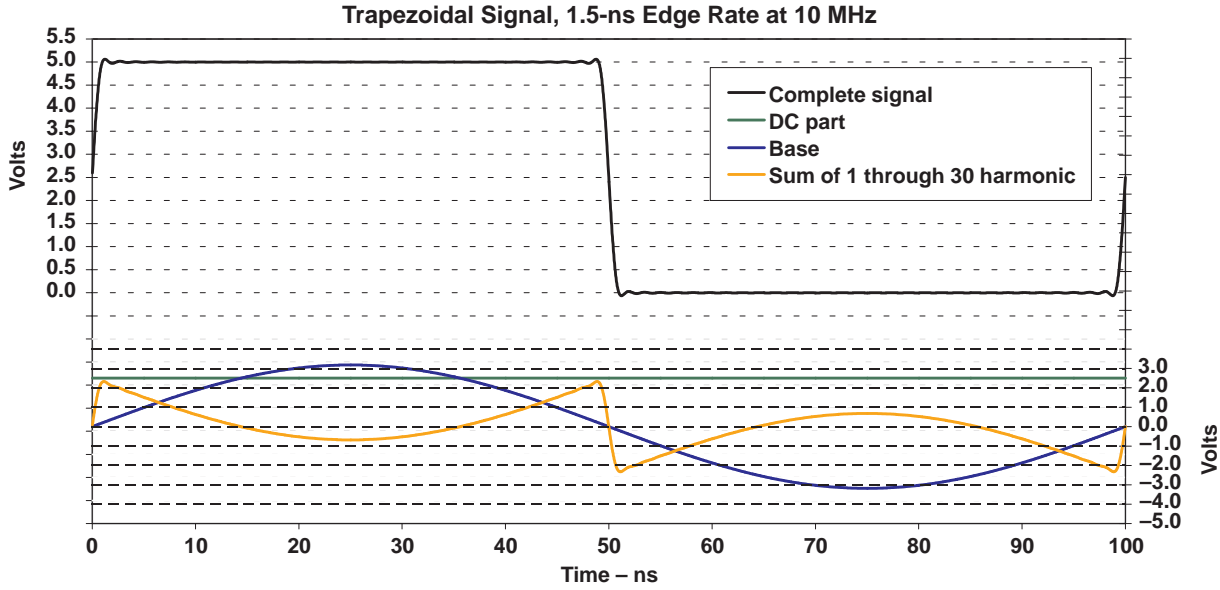


Figure 5. Spectrum for a Trapezoidal Signal, Signal and Components in Time Domain, Same Signal in Frequency Domain

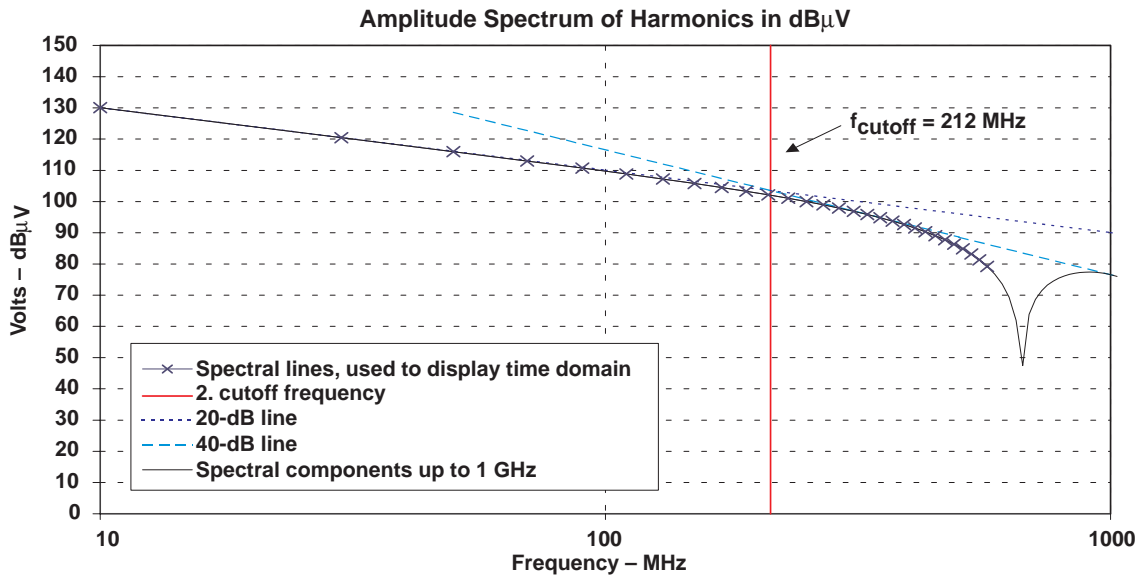


Figure 6. Spectrum for a Trapezoidal Signal (Signal From Figure 5 in Frequency Domain)

From these considerations, it directly follows that, in the case of a steeper slope, the higher-frequency-spectrum components are contained with higher amplitudes. This consideration is confirmed by Fourier-series development. In the case of the triangular signal, the 20-dB range is not even recognizable because the transition from 20 dB to 40 dB per decade occurs with $t_{r,f} = 50$ ns at 6.37 MHz, according to equation 13. Figure 4 shows that the first harmonic of the triangular signal at 20 MHz is on the 40-dB attenuation line and, therefore, is clearly attenuated.

In the comparison above, signal amplitude is set as 5 V in both cases. This amplitude corresponds to typical 5-V CMOS drivers. However, with modern technologies, lower-level definitions are employed. The reasons are power saving, more reliable signal analysis of voltage levels, and lower interference potential. Table 1 shows typical parameters for various technologies for data transmission. In addition to the switching thresholds and voltage swings, the typical values for signal slopes of output stages and maximum cycle frequency also are given.

Table 1. Comparison of Signal Levels Among Various Technologies

PARAMETER	5-V CMOS	LVTTTL	BTL	GTL	LVDS
Supply voltage	5 V	3.3 V	5 V	3.3 V od. 5 V	3.3 V
V_{IL}	1.5 V	0.8 V	1.47 V	$V_{REF} + 50$ mV	0.8 V
V_{IH}	3.5 V	2.0 V	1.62 V	$V_{REF} - 50$ mV	2.0 V
V_{OL}	0.1 V	0.1 V	0.75 V	0.55 V	247 mV to 454 mV Typ 340 mV†
V_{OH}	4.9 V	3.2 V	2.1 V	1.2 V/1.5 V	†
Rise/decay time	~2.5 ns	~2 ns	≥2 ns	~2 ns	500 ps
Maximum frequency	90 MHz	150 MHz	150 MHz	160 MHz	400 MHz

† For differential technologies, there are no static output levels referred to ground.

The following statements can be made:

- The greater the signal voltage swing, the higher the amplitudes of the spectrum components.
- The smaller the period duration of the signal, the higher the frequency range in which spectrum lines arise.
- The shorter the rise/decay time, the slower the spectrum components of the signal decay.

Thus, the values shown in Table 2 for the first harmonic are calculated, taking account of the parameters of voltage rise and fall times inherent in this technology for a periodic signal with 10-MHz frequency.

Table 2. Calculated Amplitudes of Harmonics for Various Technologies

TECHNOLOGY	AMPLITUDE OF 1ST HARMONIC (dB μ V)	CUTOFF FREQUENCY (MHz)	SPECTRUM COMPONENT AT 490 MHz (25th HARMONIC) (dB μ V)
5-V CMOS	120.08	63.66	80.8
LVTTL	116.31	79.58	58.8
GTLP	107.33	79.58	49.3
GTL	104.57	79.58	46.5
BTL	106.48	79.58	67.4
LVDS	92.55	318.3	48.5

The technology with the smallest voltage swing also is the technology that has the lowest amplitude of the first harmonic.

It also is worth noting the curve of the spectrum lines. The 40-dB-per-decade cutoff frequency for a signal with longer rise and fall times is lower than that of a signal with a steeper slope.

The cutoff frequency is calculated according to equation 13 for LVDS devices at 318 MHz, while, for the other technologies, the cutoff frequency is 60 MHz to 80 MHz. This is due to the very short rise/decay times for the LVDS drivers, stated as 500 ps in the data sheets.

Figure 7 illustrates the complete curve of the spectrum components of a 10-MHz signal for 5-V CMOS, 3.3-V LVTTL, BTL, GTL, and LVDS signals for 10 MHz to 1 GHz. In this context, we have taken into account the varying rise/fall times.

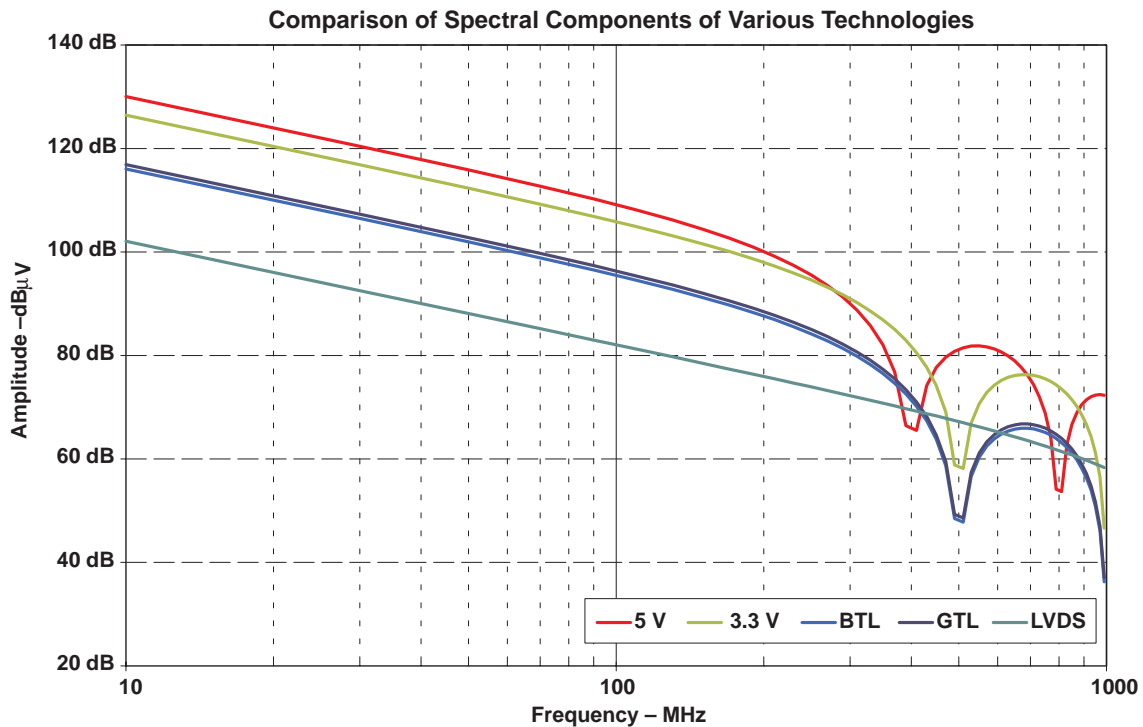
**Figure 7. Comparison of Various Technologies' Harmonics**

Figure 7 shows ranges where the harmonics of a signal with a higher switching level have a lower value than a signal with a lower switching level. Thus, the spectrum components of the LVDS signal, despite the lower voltage rise, reside in the range of 400 MHz to 600 MHz higher in this theoretical study than GTL and BTL signals. Even the 5-V CMOS signal includes ranges with lower values for the harmonic than the LVDS technology.

Measurement of the Harmonic Contents of a Digital Signal

It is possible to measure electromagnetic interference potential using various methods. Two common methods are the line-related method and measurement methods using a transverse electromagnetic mode (TEM) measurement cell. While in the case of the line-related measurement methods the interference potential is measured directly at the output of the device under test (DUT), with the TEM-cell method, the electromagnetic field within the measurement cell, which is generated by the test device, is measured.

Texas Instruments has released an application report concerning the line-related measurement method. Results reported indicate good correlation with the theoretical considerations set out in the first section of this application report.

Measurement of the Amplitude Spectrum in the TEM Cell

Using a TEM measurement cell, the entire electromagnetic field generated by a module can be measured. Figure 8 shows the test setup for the measurement.

A DUT in the measurement cell is actuated using the power-supply voltage specified for it and the signal levels applicable to it. One output is operated at a time. Switching frequency is 10 MHz at a duty cycle of 50%.

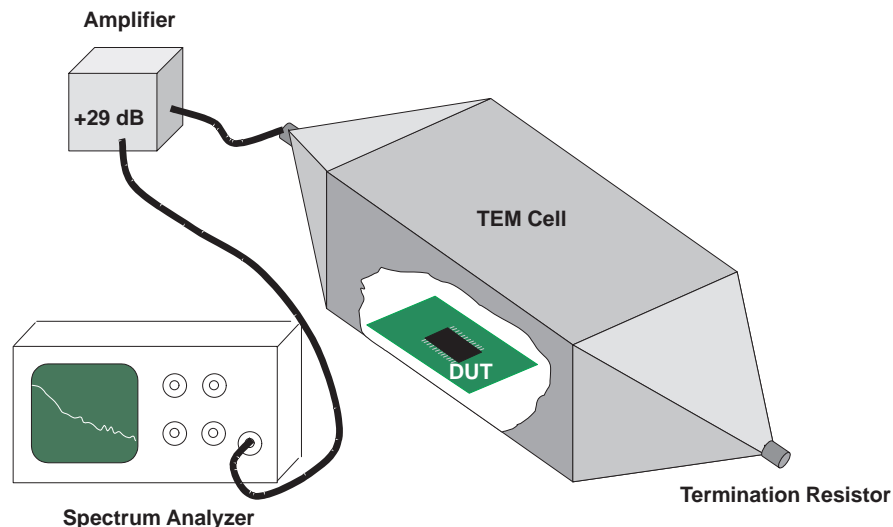


Figure 8. Measurement of the Electromagnetic Field Using a TEM Cell

The septum of the TEM cell detects the electromagnetic field generated by the DUT.

An amplifier (Advantest R 14601) provides preamplification, by 29 dB, in the range from 9 kHz to 1 GHz. The cascaded spectrum analyzer (Rhode & Schwartz FSEA 20/30) then examines the amplified signal for its spectral components. The spectrum analyzer provides the result in dBm. The dBm value can be converted into dB μ V, using equation 14. The formula accounts for the 50- Ω environment, preamplifier, and distance from the DUT to the septum.

$$x(\text{dB}\mu\text{V}/\text{meter}) = 20 \log \left[\frac{\sqrt{50\Omega \times 10^{-3} \text{ W} \times 10^{\frac{x(\text{dBm}) - 29 (\text{dBm})}{10}}}}{10^{-6} \text{ V} \times 0.043 \text{ m}} \right] \quad (14)$$

During measurement with TEM cells, all frequencies within the measurement range that are generated or irradiated by the integrated switching circuit in the form of electromagnetic waves are detected.

In the process of measurement, no distinction was drawn between electromagnetic radiation generated from the power supply currents and electromagnetic radiation generated by the output signal.

The actuation signal at the DUT input also controls a component of the spectrum. Although it is possible to examine exclusively the output signal using competitive measurements, in practice, there is no means to fade out the input interference potential.

Measurement Boards

Four-layer printed circuit boards (PCBs) were produced for the measurement. The layer structure is illustrated in Figure 9. On the side of the PCB facing the TEM cell, there is only the module to be examined (DUT); the other side is filled in as the grounding plane. All necessary actuation signals and feed lines to the measurement panel are on the outside of the circuit-board-actuation side of the TEM measurement cell.

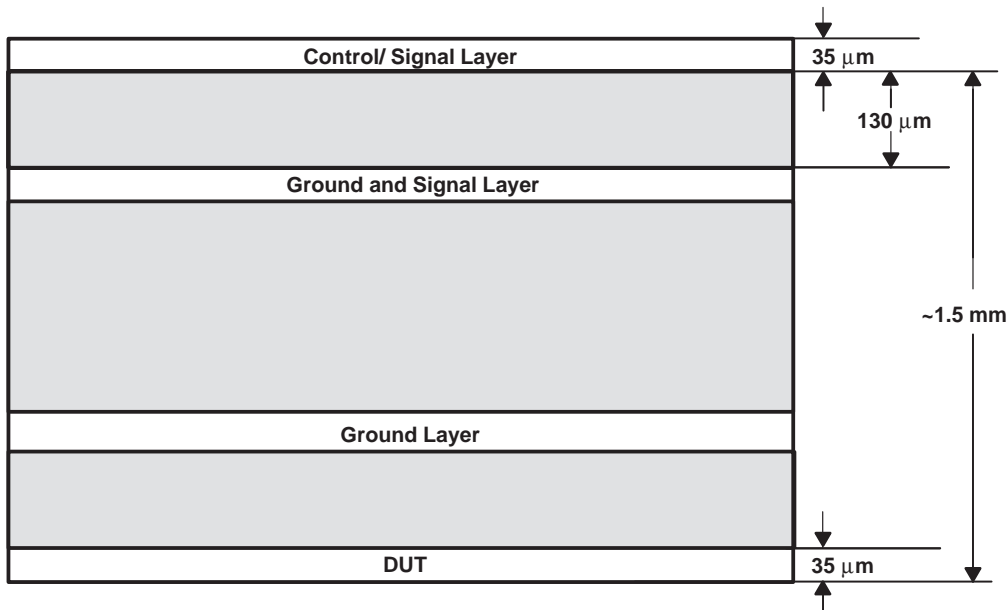


Figure 9. Layer Structure of Measurement Boards for the TEM Cell

In the design of the measurement board, all through contact points from the control layer to the DUT side were routed in the contact surfaces of the DUT pins. Investigations have shown that, by this means, it is possible to minimize inhomogeneities in the track guidance and, thus, minimize additional sources for radiation.

Measurement Results

The spectra in Figures 10–33 consist of the output signal generated by the DUT and the actuation signal, which is at the input of the probe. The devices' input signal was 10 MHz for all measurements.

In order to measure the influence of the actuated signal, two different rise and fall times were selected for measurement: $t_{r,f} = 2$ ns and 10 ns.

The following modules were examined for comparison:

- SN74AVC16244, as an example of CMOS technology, operated at 3.3 V and 1.2 V
- SN74FB2033A, as an example of backplane transceiver logic
- SN74GTLP1655, as an example of Gunning transceiver logic
- SN65LVDS31, as an example of low-voltage differential signaling

Measurement results illustrate both the oscilloscope signal and the frequency spectrum recorded by the spectrum analyzer.

AVC16244

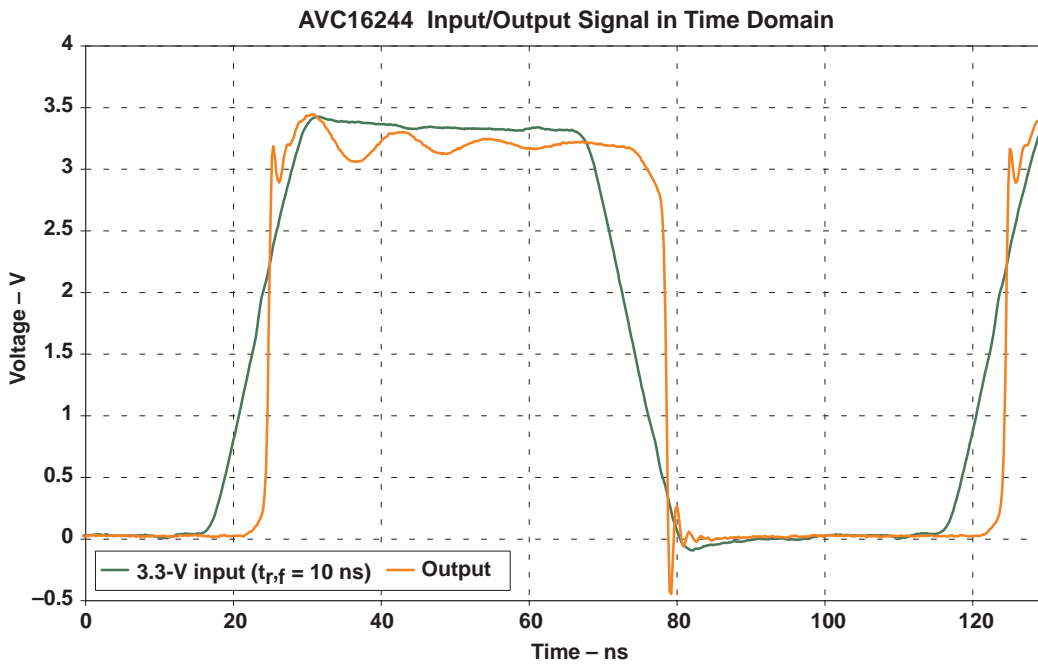


Figure 10. Input and Output Signals of AVC16244, $V_{CC} = 3.3$ V, $f = 10$ MHz, Input Signal LVTTTL $t_{r,f} = 10$ ns; Output Signal LVTTTL

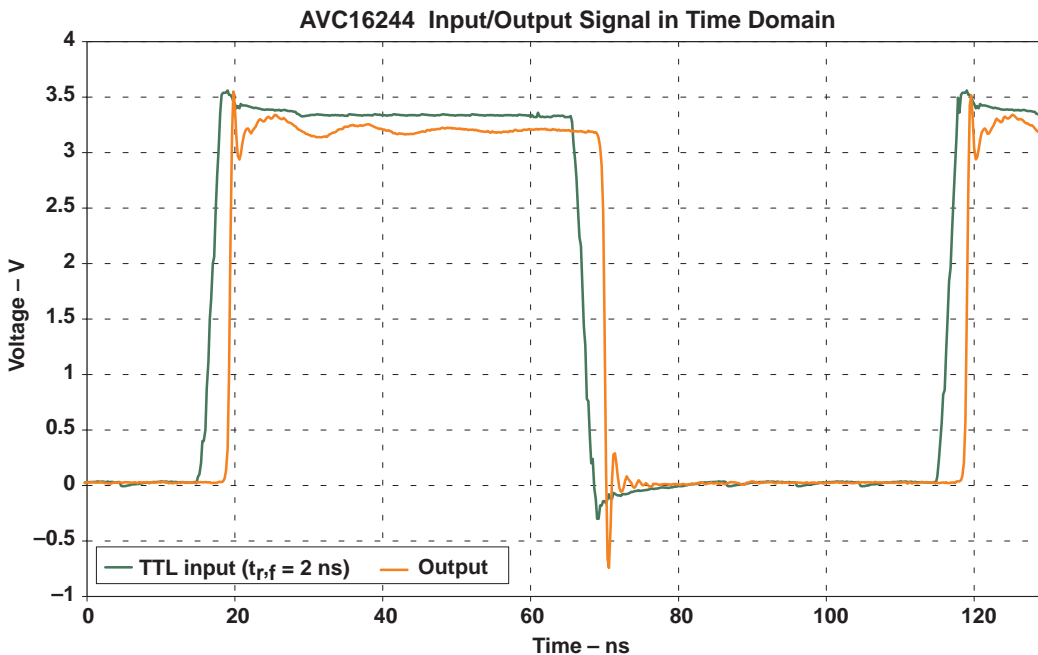


Figure 11. Input and Output Signals of AVC16244, $V_{CC} = 3.3$ V, $f = 10$ MHz, Input Signal LVTTTL $t_{r,f} = 2$ ns; Output Signal LVTTTL

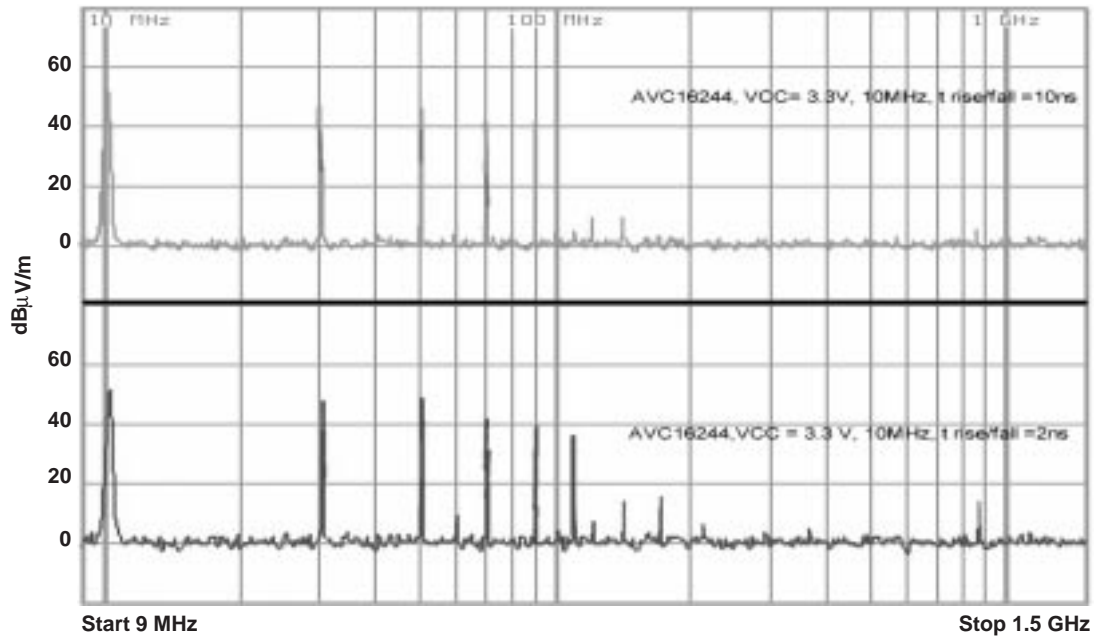


Figure 12. Spectrum Measured in the TEM Cell, AVC16244, $V_{CC} = 3.3\text{ V}$, $f = 10\text{ MHz}$

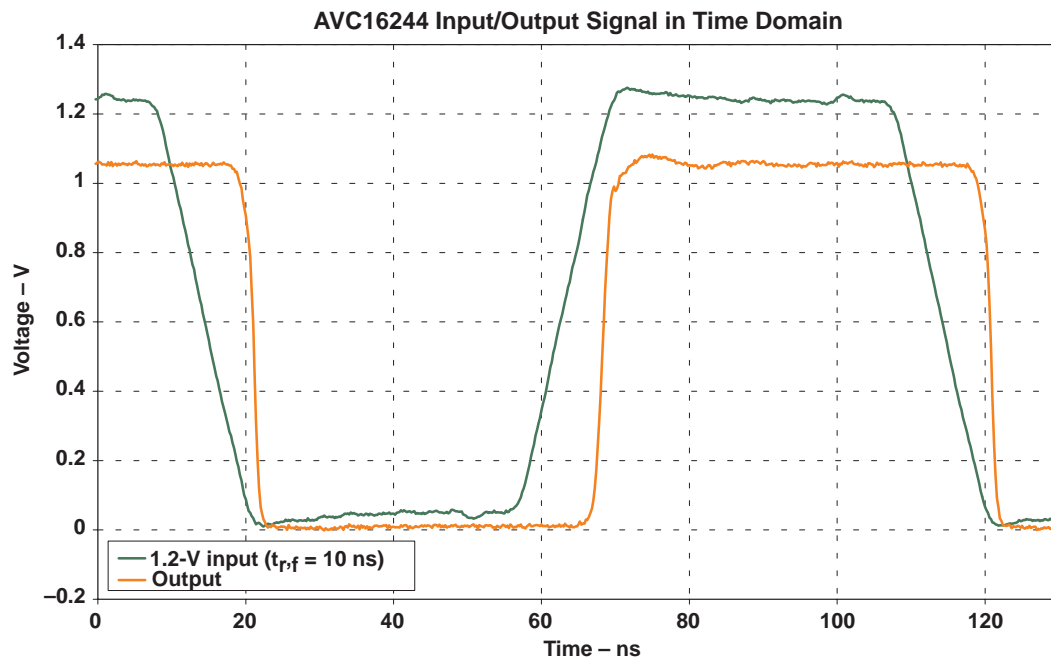


Figure 13. Input and Output Signals of AVC16244, $V_{CC} = 1.2\text{ V}$, $f = 10\text{ MHz}$; Input Signal 1.2 V, $t_{r,f} = 10\text{ ns}$; Output Signal 1.2-V CMOS

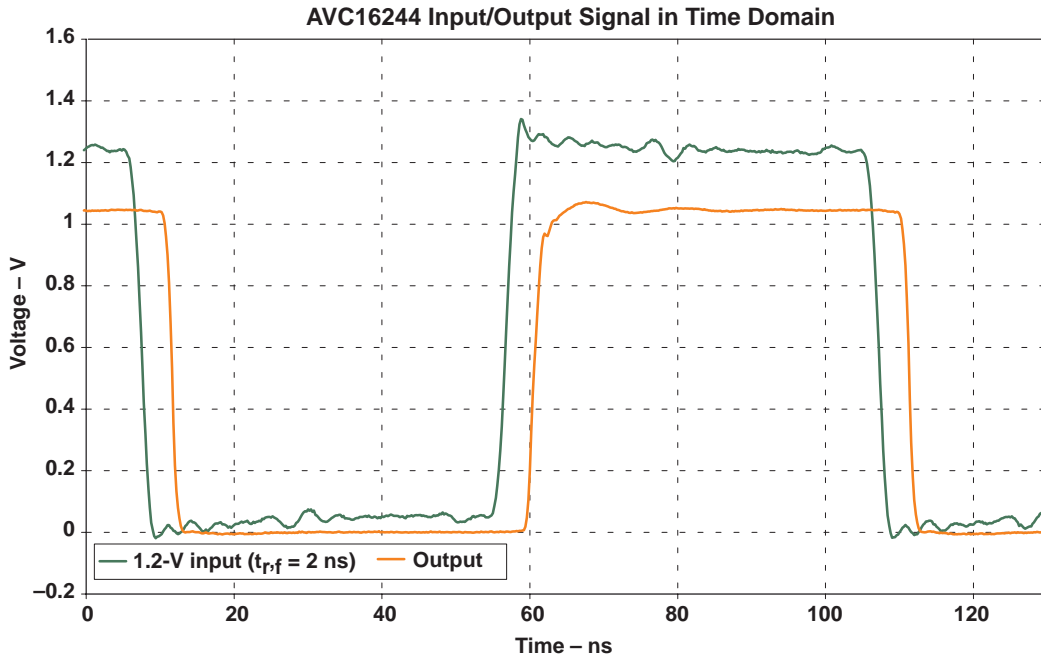


Figure 14. Input and Output Signals of AVC16244, $V_{CC} = 3.3\text{ V}$, $f = 10\text{ MHz}$, Input Signal 1.2 V, $t_{r,f} = 2\text{ ns}$; Output Signal 1.2-V CMOS

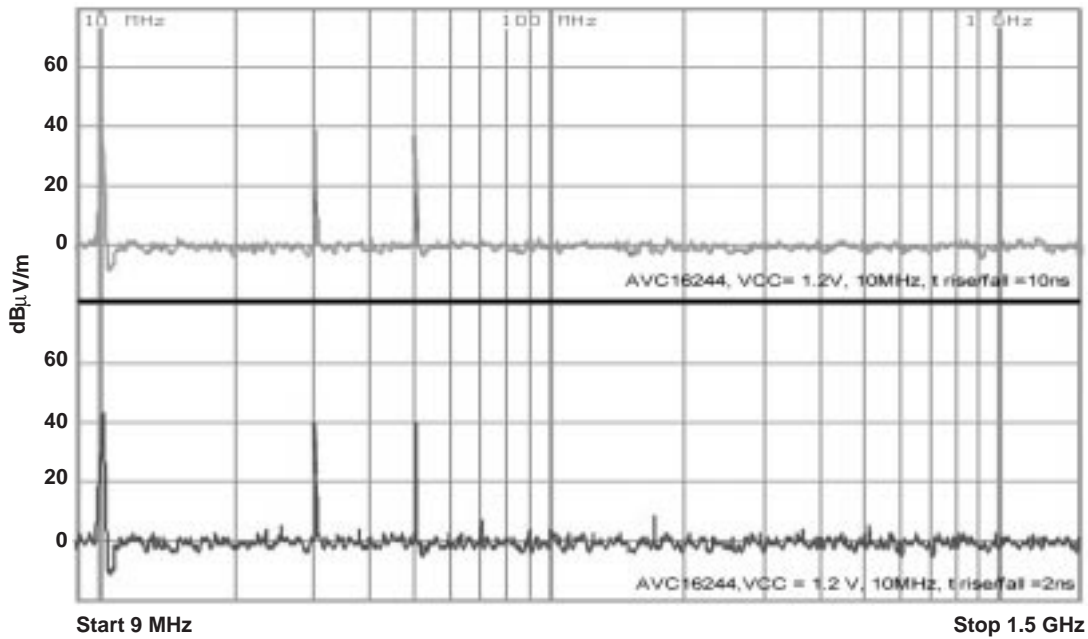


Figure 15. Spectrum Measured in the TEM Cell, AVC16244, $V_{CC} = 1.2\text{ V}$, $f = 10\text{ MHz}$

FB2033A

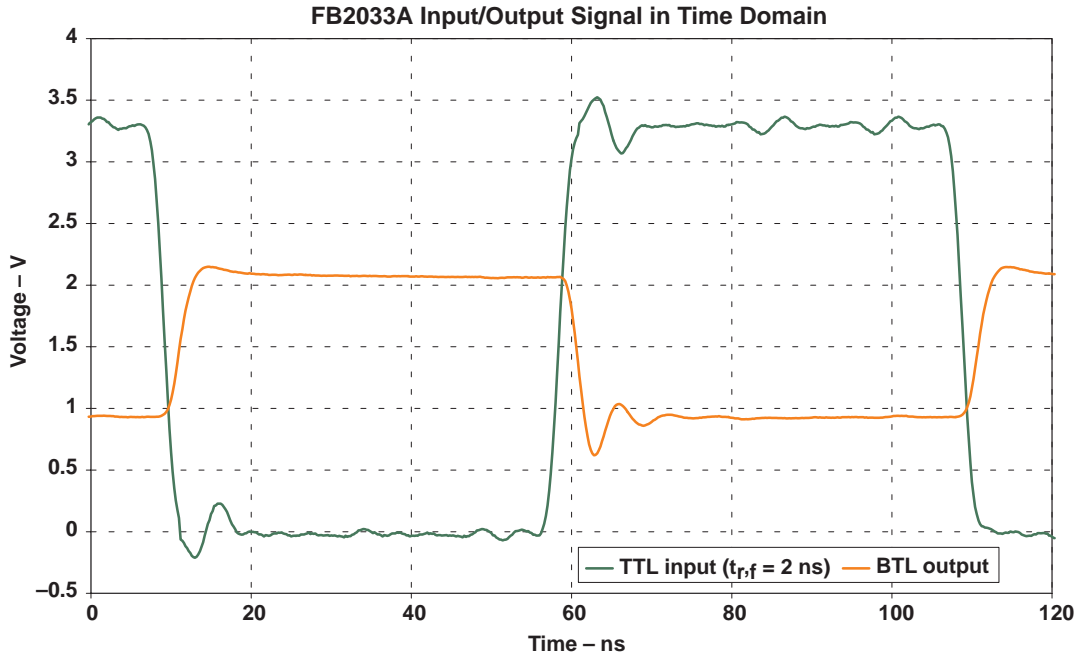


Figure 16. Input and Output Signals of FB2033A, $f = 10$ MHz, Input Signal LVTTTL, $t_{r,f} = 2$ ns; Output Signal BTL

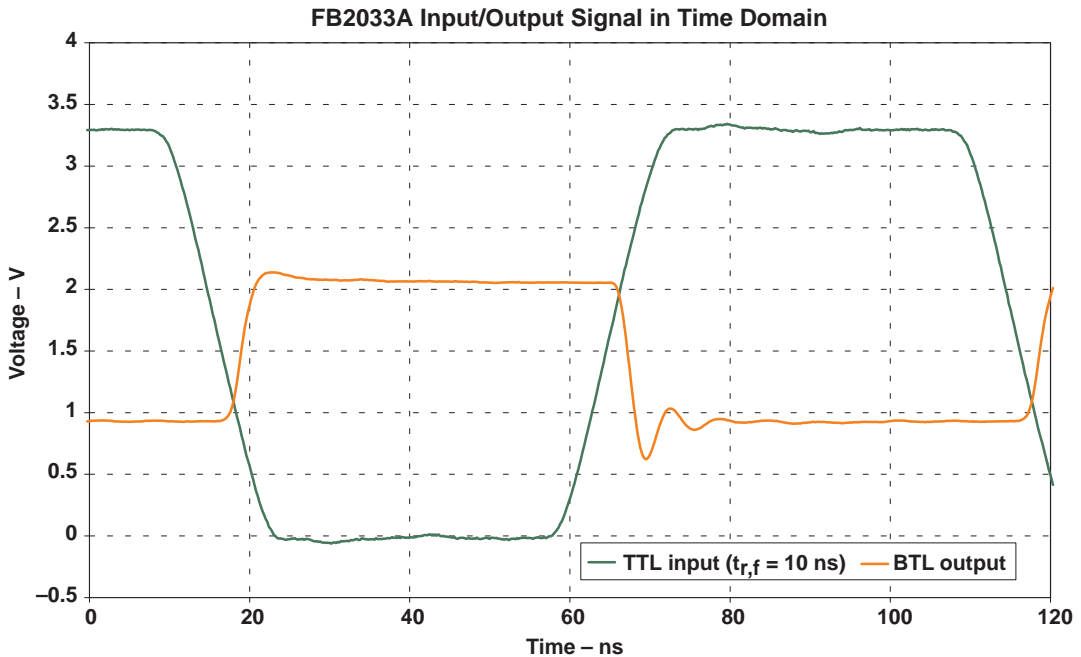


Figure 17. Input and Output Signals of FB2033A, $f = 10$ MHz, Input Signal LVTTTL, $t_{r,f} = 10$ ns; Output Signal BTL

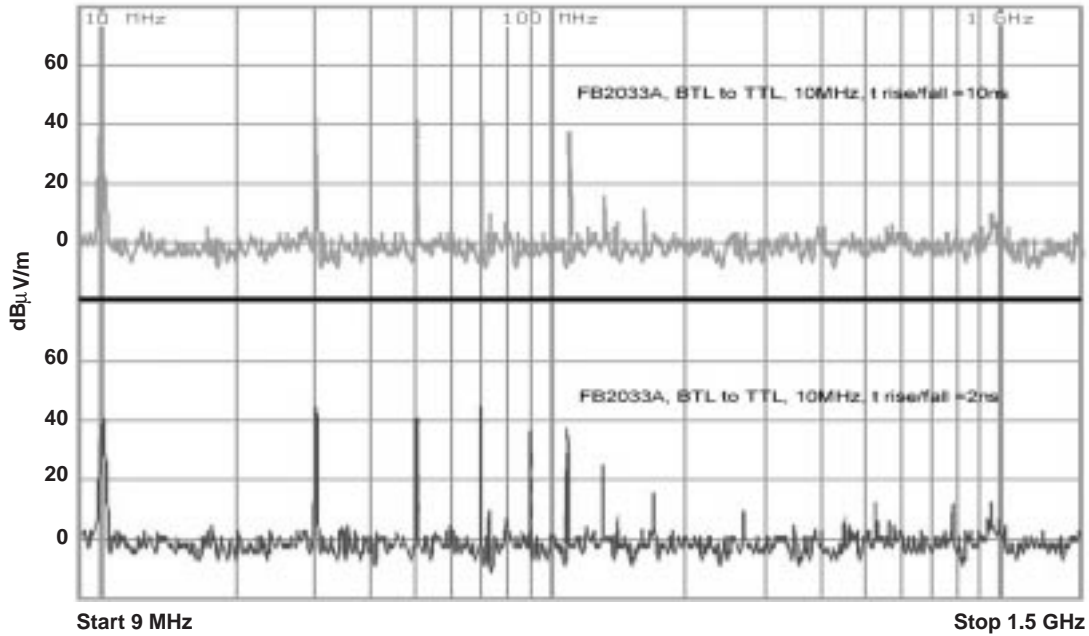


Figure 18. Spectrum Measured in the TEM Cell, FB2033A, $f = 10$ MHz, Input Signal BTL; Output Signal LVTTTL

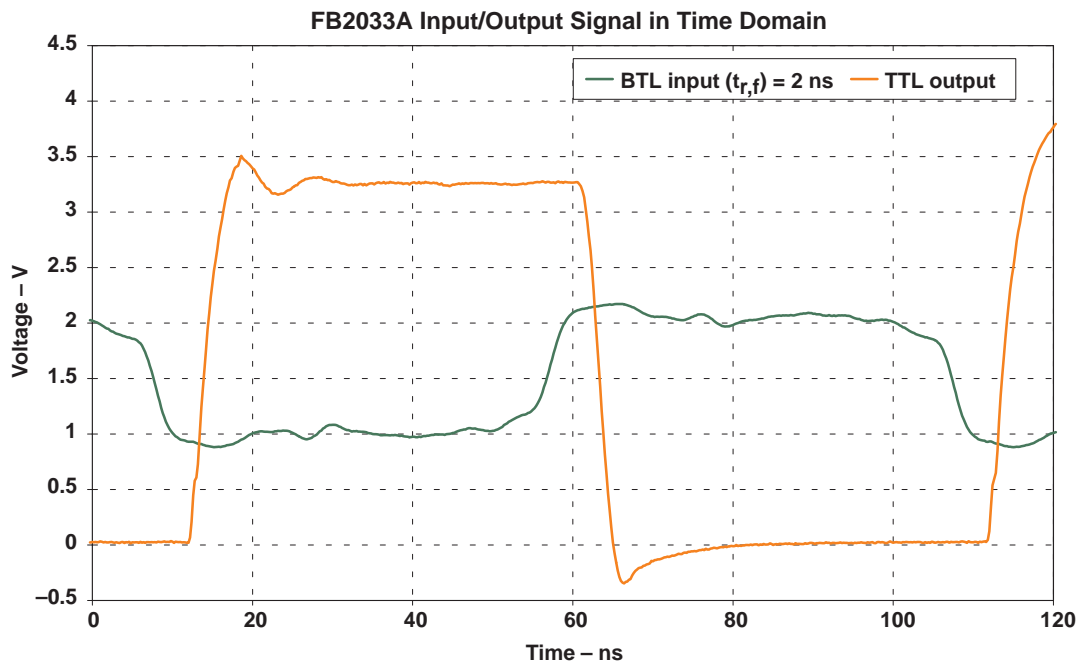


Figure 19. Input and Output Signals of FB2033A, $f = 10$ MHz; Input Signal BTL, $t_{r,f} = 2$ ns; Output Signal LVTTTL

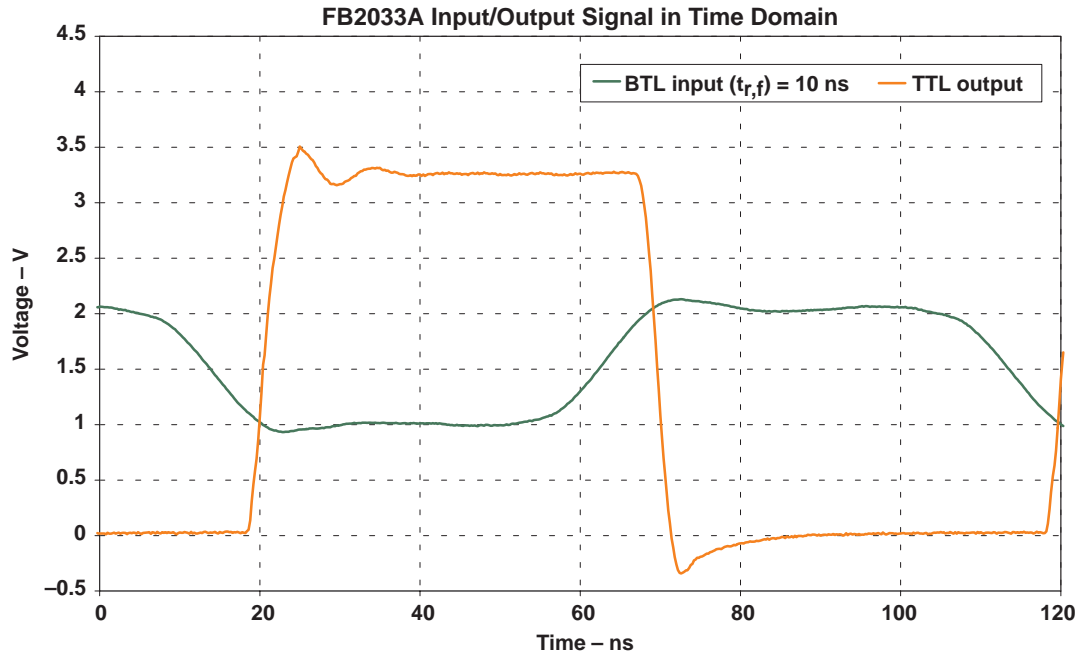


Figure 20. Input and Output Signals of FB2033A, $f = 10 \text{ MHz}$, Input Signal BTL, $t_{r,f} = 10 \text{ ns}$; Output Signal LVTTTL

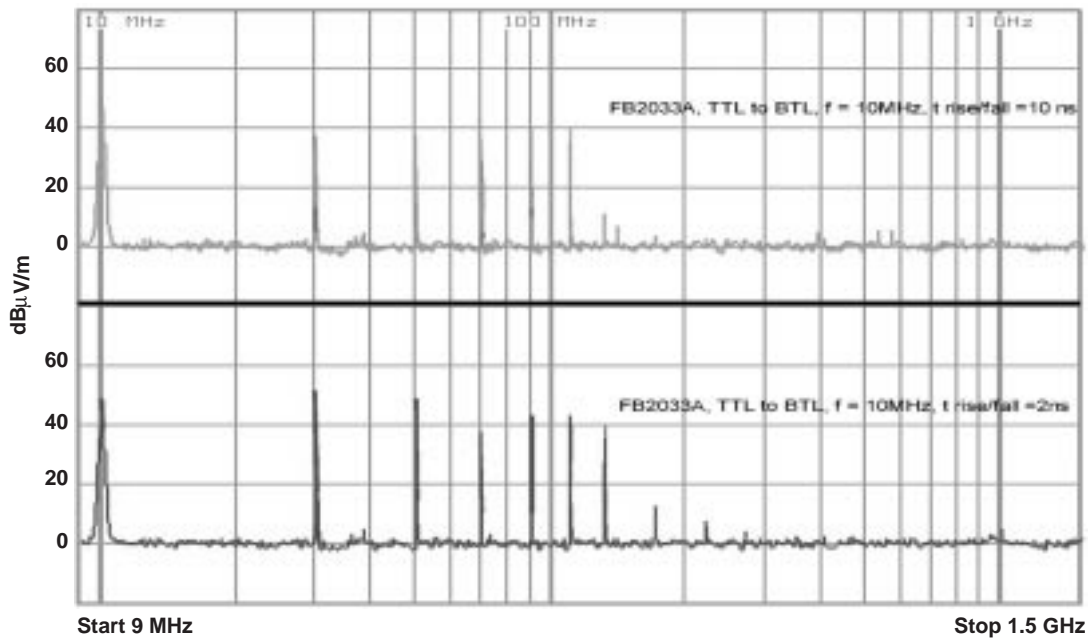


Figure 21. Spectrum Measured in the TEM Cell FB2033A, $f = 10 \text{ MHz}$, Input Signal LVTTTL; Output Signal BTL

GTLPH1655

A particular feature of the GTLPH1655 is the option to vary the GTL driver's output rise and fall times between slow and fast. This enables optimum dynamic adaptation to load and speed in the application.

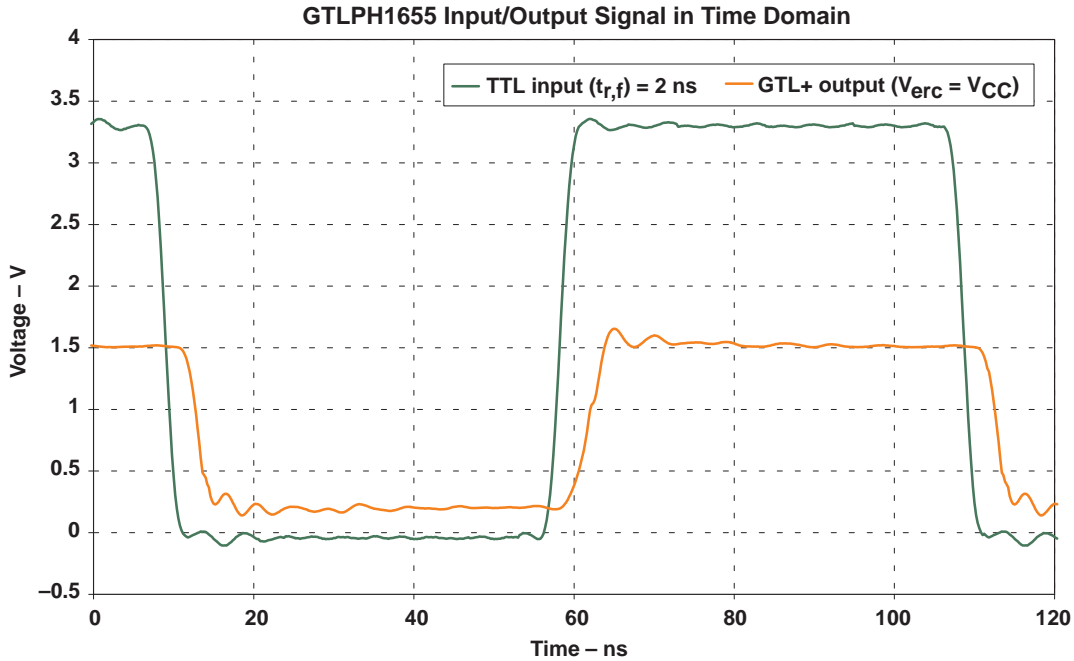


Figure 22. Input and Output Signals of GTLPH1655, $f = 10$ MHz, Input Signal LVTTTL, $t_{r,f} = 2$ ns; Output Signal GTL+ With Slow Edge Rate

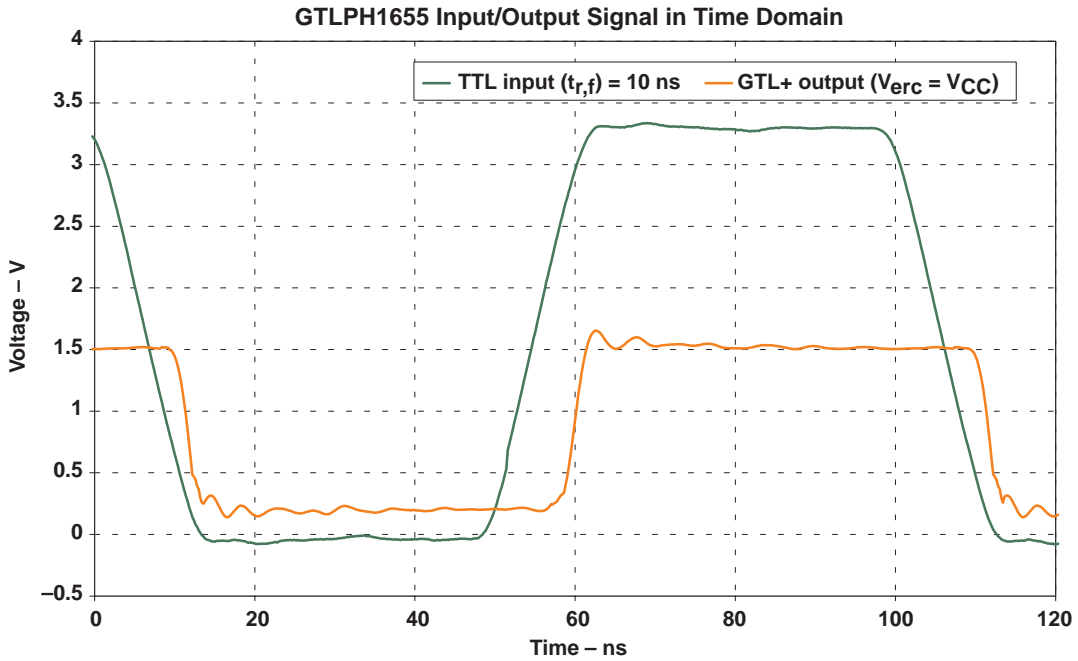


Figure 23. Input and Output Signals of GTLPH1655, $f = 10$ MHz, Input Signal LVTTTL, $t_{r,f} = 10$ ns, Output Signal GTL+ With Slow Edge Rate

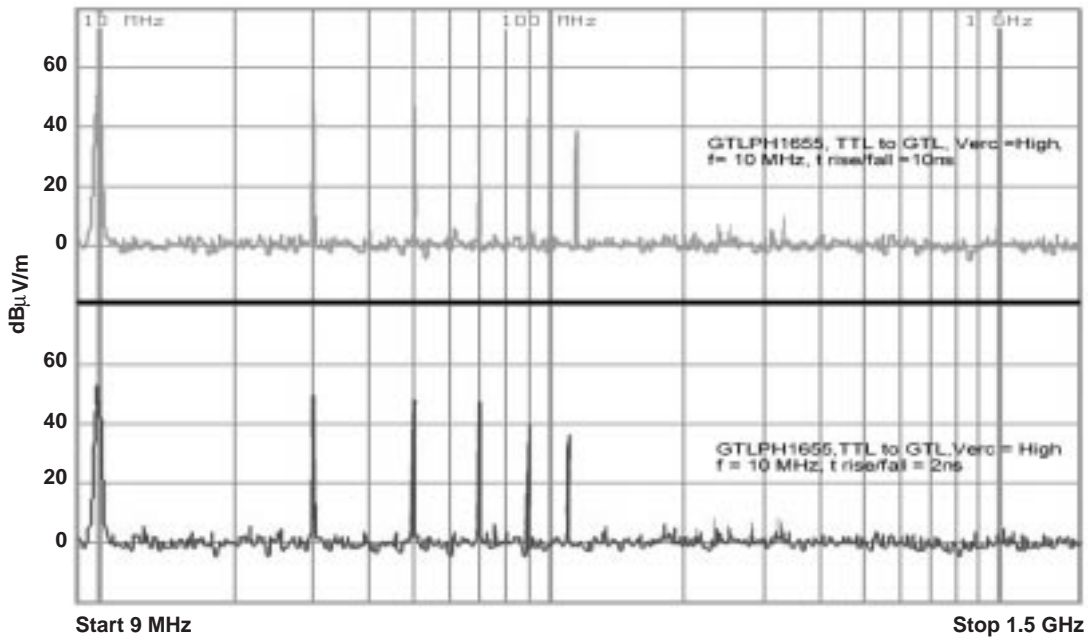


Figure 24. Spectrum Measured in the TEM Cell, GTLPH1655 $f = 10$ MHz, Input Signal LVTTTL; Output Signal GTL+ With Slow Edge Rate

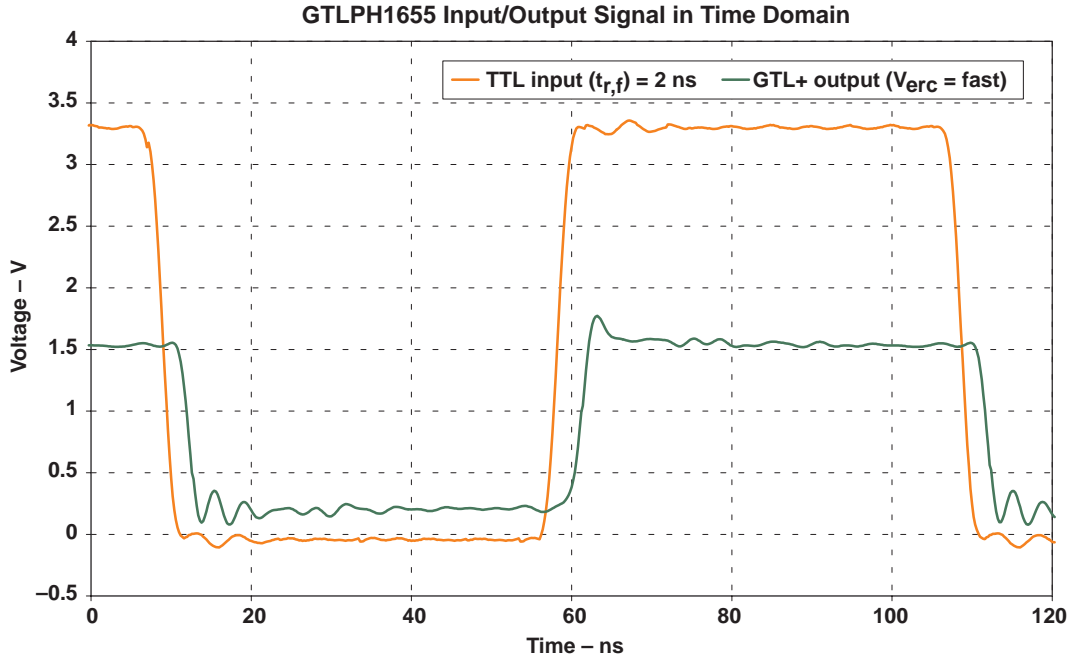


Figure 25. Input and Output Signal of GTLPH1655, $f = 10$ MHz, Input Signal LVTTTL, $t_{r,f} = 2$ ns; Output Signal GTL+ With Fast Edge Rate

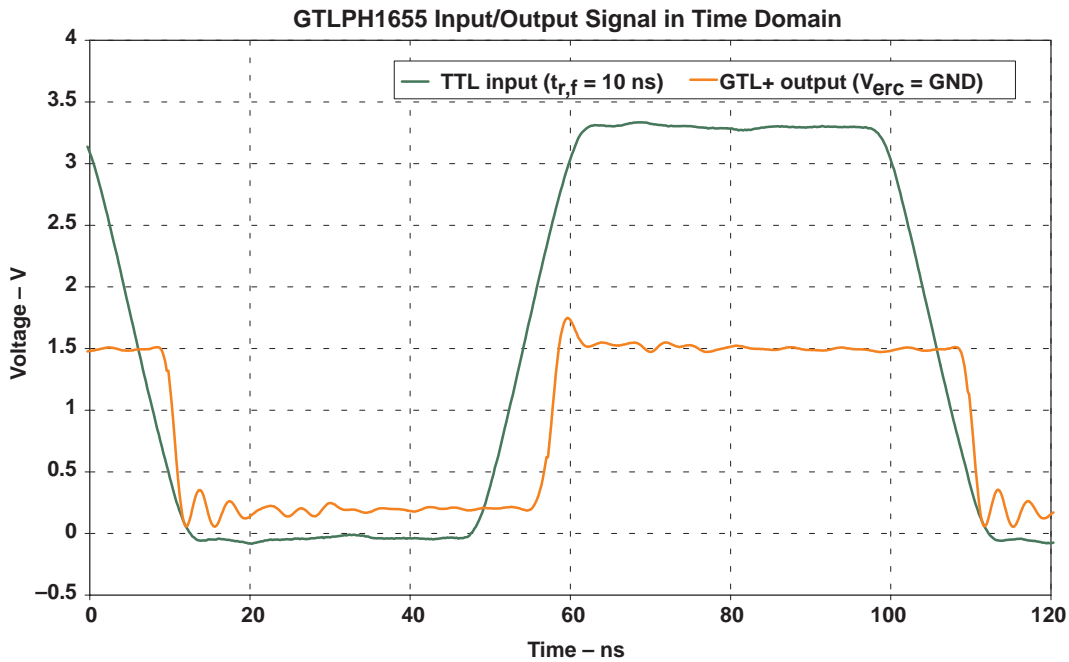


Figure 26. Input and Output Signals of GTLPH1655, $f = 10$ MHz, Input Signal LVTTTL, $t_{r,f} = 10$ ns; Output Signal GTL+ With Fast Edge Rate

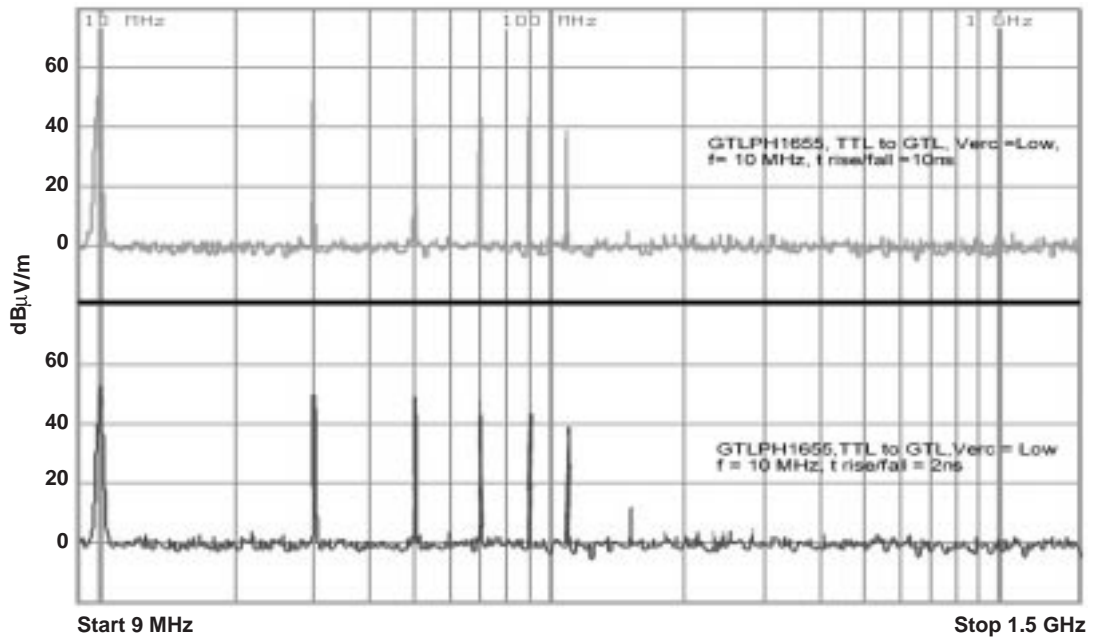


Figure 27. Spectrum Measured in the TEM Cell for GTLPH1655, $f = 10$ MHz, Input Signal LVTTL; Output Signal GTL+ With Fast Edge Rate

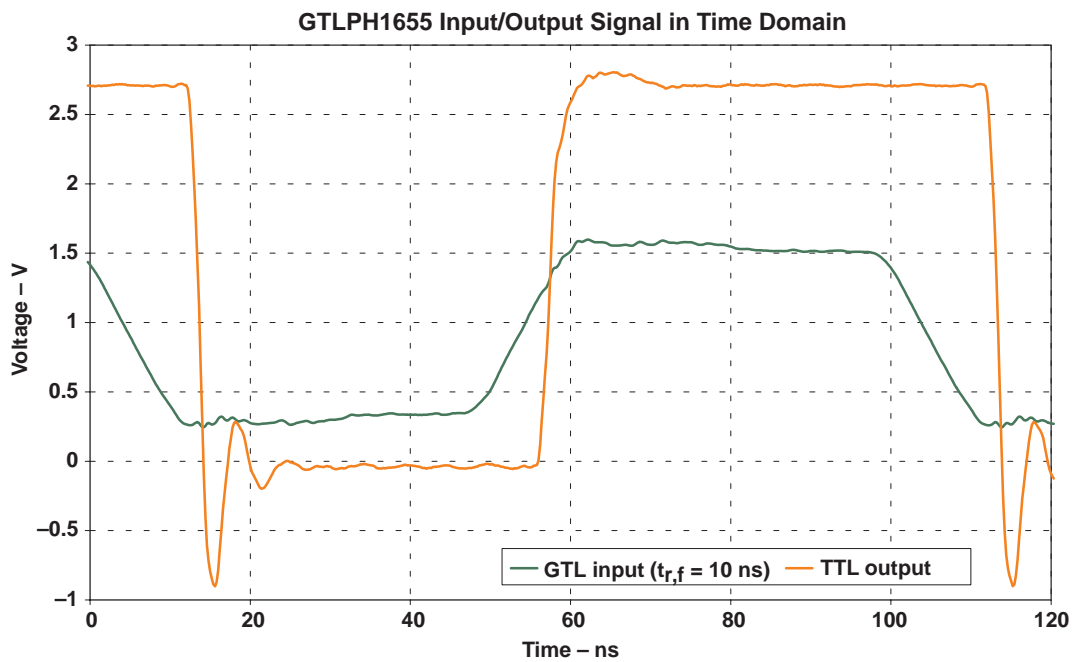


Figure 28. Input and Output Signals of GTLPH1655, $f = 10$ MHz, Input Signal GTL+, $t_{r,f} = 10$ ns; Output Signal GTL+ LVTTL

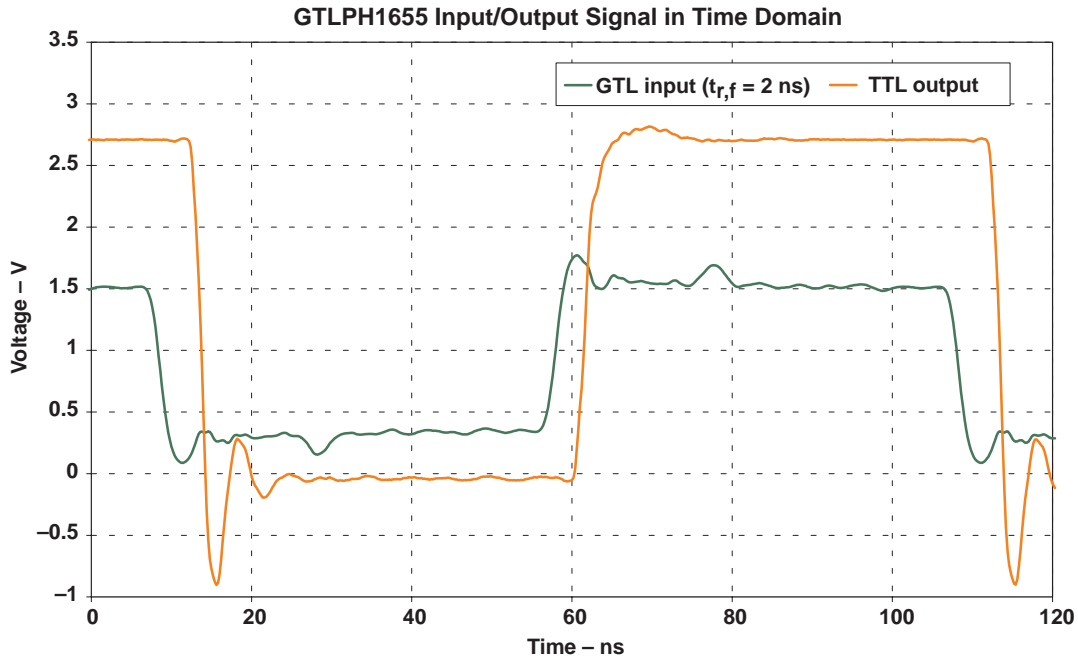


Figure 29. Input and Output Signal of GTLPH1655, $f = 10 \text{ MHz}$, Input Signal GTL+, $t_{r,f} = 2 \text{ ns}$; Output Signal LVTTTL

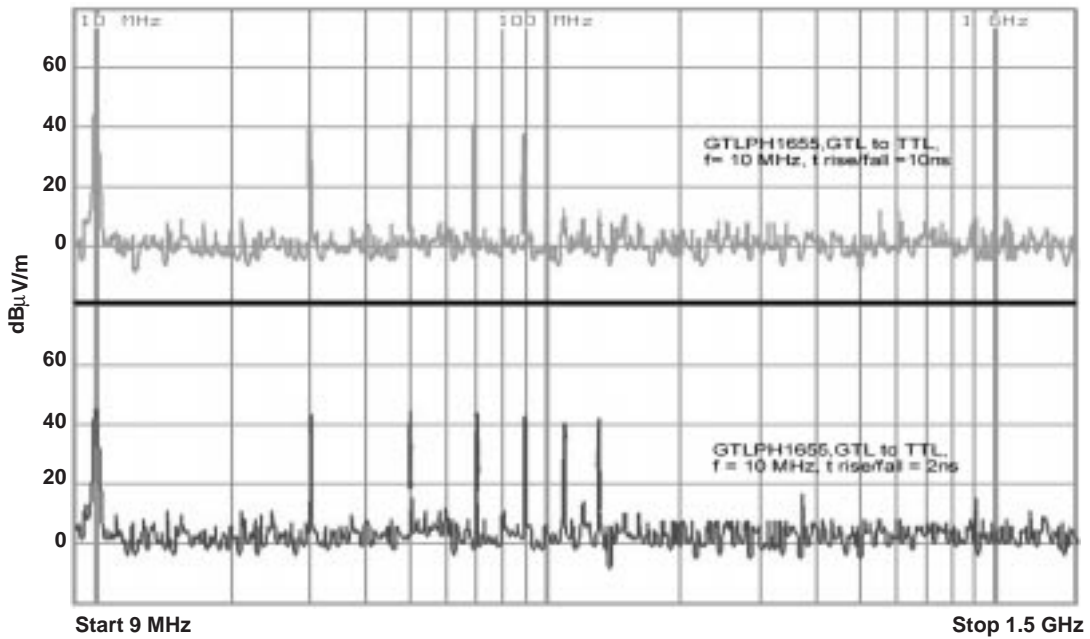


Figure 30. Spectrum Measured in the TEM Cell for GTLPH1655, $f = 10 \text{ MHz}$, Input Signal GTL+; Output Signal LVTTTL

LVDS31

The LVDS31 module is the only representative of differential technology in this comparison. Consequently, measurements with the oscilloscope at the module output were performed using a differential probe.

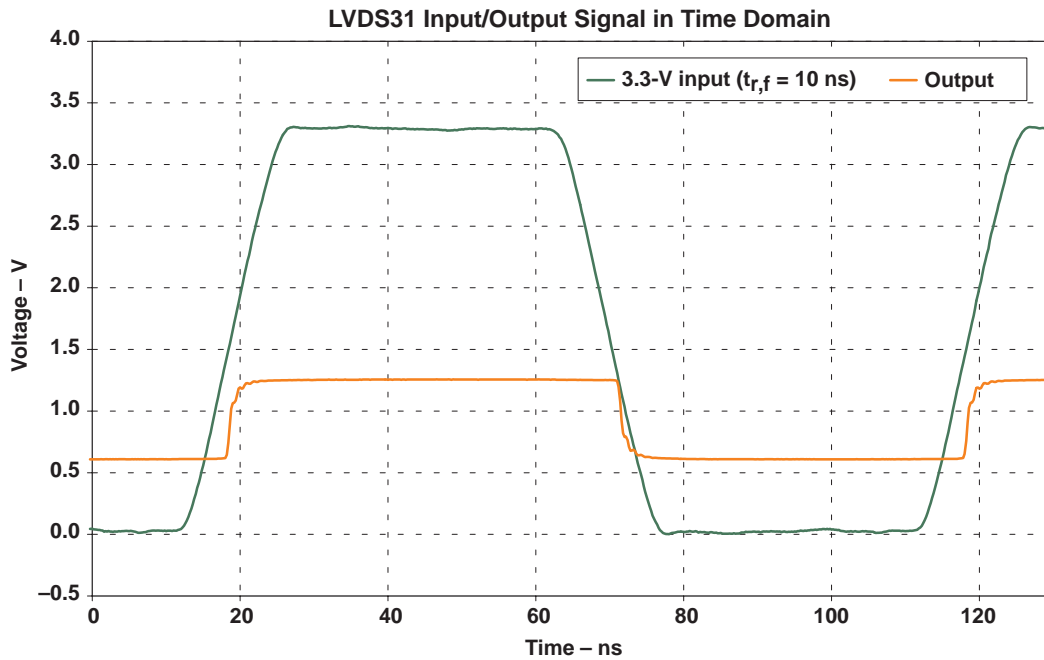


Figure 31. Input and Output Signals of LVDS31, $f = 10$ MHz, TTL Input Signal, $t_{r,f} = 10$ ns; Output Signal LVDS

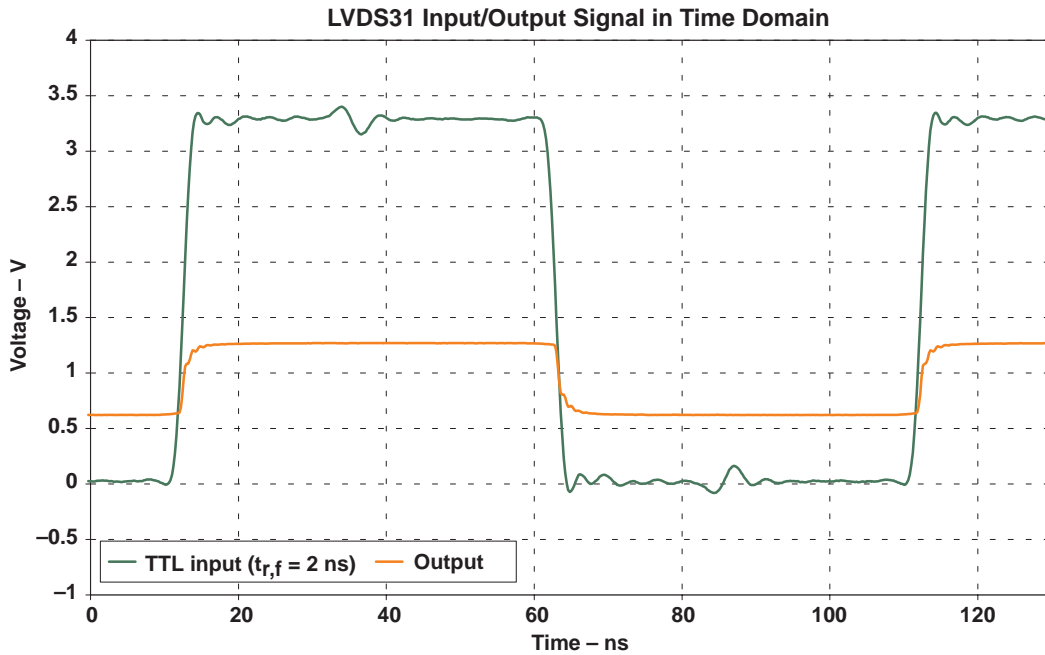


Figure 32. Input and Output Signals of LVDS31, $f = 10 \text{ MHz}$, Input Signal TTL, $t_{r,f} = 2 \text{ ns}$; Output Signal LVDS

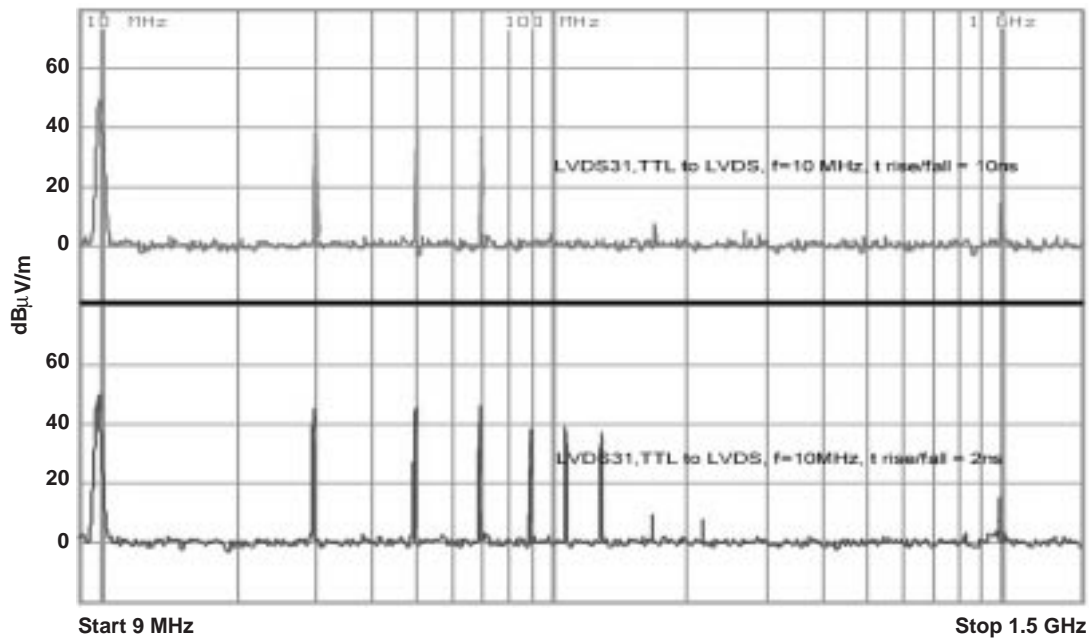


Figure 33. Spectrum Measured in the TEM Cell for LVDS31, $f = 10 \text{ MHz}$, Input Signal TTL; Output Signal LVDS

Summary

The trend toward development of new systems for data transmission is continuing, unchanged, toward lower supply voltages. The advantages of lower supply voltages not only are lower power consumption and the option to create smaller structures, but also, as illustrated most clearly in the context of the example of the AVC module, lower electromagnetic radiation.

All other technologies investigated in this context (BTL, GTL, and LVDS) operate as translators between the respectively specified logic levels at one port side and LVTTTL levels at the other port connection. With regard to electromagnetic radiation, however, these modules produce poor characteristics in comparative measurements using the TEM cell. However, this result can be explained by the principal measurement setup. By contrast with the line-related measurement method, in the TEM cell the signal at the input to the DUT also is what is detected. On the basis of actuation by the LVTTTL signal, a much higher spectrum is obtained than in the case of actuation by a 1.5-V CMOS signal.

To account for all spectrum components, the DUT should have rotated through 360 degrees during measurement, and each frequency's maximum spectrum components determined by that means, whereas, this is not possible using the Fischer TEM cell that was employed. However, with regard to the illustrated measurement results, it is important to note that measurements were performed only in the most unfavorable position of the measurement cell (of four possible positions), thus producing the highest measured harmonic content.

Use of the technology with the lowest electromagnetic potential does not, by itself, ensure interference-free operation.

However, awareness of the possible antenna effect of the layout and using suitable remedies, such as additional lines, shorter lines, and correct line termination to minimize electromagnetic propagation and radiation, provide very good prospects for a successful design that is free of electromagnetic interference.

Glossary

AVC	Advanced very-low-voltage CMOS
BTL	Backplane transceiver logic
CMOS	Complementary symmetry metal-oxide semiconductor
DUT	Device under test
dB	A common unit of measurement or reference. The basic unit of measurement is the logarithmic ratio between two products.
dBm	$10 \log (\text{power/mW})$
dB μ V	$20 \log (\text{volt}/1 \mu\text{V})$
EMC	Electromagnetic compatibility
EMI	Electromagnetic interference
FB	Future bus, device identifier for backplane transceiver logic devices
GND	Ground
GTLP	Gunning transceiver logic plus
I/O	Input/output
LVTTTL	Low-voltage transistor-transistor logic supplied with 3.3-V, compatible TTL
LVDS	Low-voltage differential signaling
PCB	Printed circuit board
Slew rate	The slew rate is derived using the following equation: slew rate = $\Delta V/\Delta t = (0.8 V_{OH} - V_{OL})/t_{r,f}$
TEM cell	Transverse electromagnetic mode measurement cell
TTL	Transistor-transistor logic
t_{pd}	Propagation delay time
t_f	Time to transit from a logical high to logical low, measured between the 90% and 10% values of the steady logical-high level
t_r	Time to transit from a logical low to logical high, measured between the 10% and 90% values of the steady logical high level
V_{CC}	Supply voltage

Bibliography

Donald R. J. White, *EMI Control in the Design of Printed Circuit Boards and Backplanes*, Interference Control Technologies Inc.

Mark I. Montrose, *Printed Circuit Board Design Techniques for EMC Compliance*, IEEE Press Series on Electronics Technology.

Mark I. Montrose, *EMC and the Printed Circuit Board*, IEEE Press Series on Electronics Technology.

Howard Johnson, Martin Graham, *High-Speed Digital Design – a Handbook of Black Magic*, Prentice-Hall.

Texas Instruments, G. Becke, E. Haseloff, *Das TTL- Kochbuch*, (The TTL Cookbook), literature number SDYZG17.

Texas Instruments, *Automotive PCB Design for Reduced EMI*, May 1998, literature number SDYA017.

Texas Instruments, *AVC Logic Family Technology and Applications*, 1998, literature number SCEA006A.

Texas Instruments, *ABT Logic Advanced BICMOS Technology Data Book*, 1997, literature number SCBD002C.

Texas Instruments, *AVC Advanced Very Low Voltage CMOS Logic Data Book*, March 2000, literature number SCAD008B.

Texas Instruments, *Logic Selection Guide and Data Book CD-ROM*, April 1998, literature number SCBC001B.

Texas Instruments, *CBT (5-V) and CBTLV (3.3-V) Bus Switches Data Book*, 1998, literature number SCDD001B.

Texas Instruments, *AHC/AHCT Logic Advanced High-Speed CMOS Data Book*, 2000, literature number SCLD003B.

Texas Instruments, *Design Considerations for Logic Products*, 1997, literature number SDYA002.

Texas Instruments, *Digital Design Seminar – Reference Manual*, 1998, literature number SDYDE01B.

Texas Instruments, *What a Designer Should Know*, March 1997, literature number SDYA009B.

Texas Instruments, *Electromagnetic Emission from Logic Circuits*, March 1998, literature number SDZAE17.

Texas Instruments, *The Bergeron Method*, October 1996, literature number SDYA014.

Texas Instruments, *Bus-Interface Devices With Output-Damping Resistors or Reduced-Drive Outputs*, August 1997, literature number SCBA012A.

Texas Instruments, *Live Insertion*, November 1995, literature number SDYA012.

Texas Instruments, *Thin Very Small Outline Package (TVSOP)*, March 1997, literature number SCBA009C.

Texas Instruments, *Low-Voltage Logic Families*, April 1997, literature number SCVAE01A.

Texas Instruments, *Input and Output Characteristics of Digital Integrated Circuits at $V_{CC} = 5\text{-V}$ Supply Voltage*, literature number SCYA002.

IMPORTANT NOTICE

Texas Instruments and its subsidiaries (TI) reserve the right to make changes to their products or to discontinue any product or service without notice, and advise customers to obtain the latest version of relevant information to verify, before placing orders, that information being relied on is current and complete. All products are sold subject to the terms and conditions of sale supplied at the time of order acknowledgment, including those pertaining to warranty, patent infringement, and limitation of liability.

TI warrants performance of its products to the specifications applicable at the time of sale in accordance with TI's standard warranty. Testing and other quality control techniques are utilized to the extent TI deems necessary to support this warranty. Specific testing of all parameters of each device is not necessarily performed, except those mandated by government requirements.

Customers are responsible for their applications using TI components.

In order to minimize risks associated with the customer's applications, adequate design and operating safeguards must be provided by the customer to minimize inherent or procedural hazards.

TI assumes no liability for applications assistance or customer product design. TI does not warrant or represent that any license, either express or implied, is granted under any patent right, copyright, mask work right, or other intellectual property right of TI covering or relating to any combination, machine, or process in which such products or services might be or are used. TI's publication of information regarding any third party's products or services does not constitute TI's approval, license, warranty or endorsement thereof.

Reproduction of information in TI data books or data sheets is permissible only if reproduction is without alteration and is accompanied by all associated warranties, conditions, limitations and notices. Representation or reproduction of this information with alteration voids all warranties provided for an associated TI product or service, is an unfair and deceptive business practice, and TI is not responsible nor liable for any such use.

Resale of TI's products or services with statements different from or beyond the parameters stated by TI for that product or service voids all express and any implied warranties for the associated TI product or service, is an unfair and deceptive business practice, and TI is not responsible nor liable for any such use.

Also see: [Standard Terms and Conditions of Sale for Semiconductor Products](http://www.ti.com/sc/docs/stdterms.htm). www.ti.com/sc/docs/stdterms.htm

Mailing Address:

Texas Instruments
Post Office Box 655303
Dallas, Texas 75265